ICSV14
Cairns • Australia
9-12 July, 2007

SYSTEM REDUCTION IN NONLINEAR MULTIBODY DYNAMICS OF WIND TURBINES

Kristian Holm-Jørgensen[1], Søren R.K. Nielsen[1], Rune Rubak[2]

[1]Department of Civil Engineering, Aalborg University
Sohngaardsholmsvej 57, DK-9000 Aalborg, Denmark

[2]Siemens Wind Power A/S
Borupvej 16, DK-7330 Brande, Denmark

Abstract

In this paper the system reduction in nonlinear multibody dynamics of wind turbines is investigated for various updating schemes of the moving frame of reference. In one case, the moving frame of reference is updated to a stiff body, relative to which the elastic deformations are fixed at one end. In the other case, the stiff body motion is defined as the chord line connecting the end points of the beam, and the elastic deformations are simply supported at the end points.

The system reduction is performed by discretizing the spatial motion into a set of rigid body modes and linear elastic eigenmodes determined from an FE-beam model complying to the definitions of the stiff body motions. Moreover, certain nonlinear effects have been included. These encompass the non-conservative rotation of the aerodynamic load during large elastic deformations and application of the aerodynamic and inertial loads in the deformed state.

To illustrate the method a numerical example of a wind turbine blade with a length of 45m attached to a rotor shaft supported by two bearings is used. The reduced model based on a truncated modal expansion has been compared with the full FE model in both linear and nonlinear analyses. The updating based on an expansion using simply supported eigenmodes turns out to be the most favourable in reducing the displacements from the moving frame.

1. INTRODUCTION

The increasing size of wind turbine blades without a proportional increase of stiffness results in large displacements. Since the substructures are described in their own moving frame of reference large rigid body motions are extracted from the structural description whereby linear or moderate nonlinear structural theory are adequate. At extreme conditions the tip displacement of an MW turbine may exceed 20% of the blade length L for which reason geometrical nonlinearities may become important. In this respect multibody dynamics offers an appropriate way of formulating the nonlinear structural response of a wind turbine.

The regular floating frame of reference formulation has been described by several authors e.g. Nikravesh 1988, Garcia & Bayo 1993, Geradin & Cardona 2001 and Shabana 2005. Here,

it is required that no rigid body motion between a given substructure and its moving frame takes place. The origin of the moving frame is defined using a set of reference coordinates $\bar{\mathbf{x}}_c(t)$ with respect to the fixed coordinate system $(\bar{x}_1, \bar{x}_2, \bar{x}_3)$. The rotation of the moving frame of reference relative to the global coordinate system is defined by the rotation tensor $\mathbf{R}(\boldsymbol{\theta})$ where $\boldsymbol{\theta}$ is a parameter vector. The elastic displacements $\mathbf{u}(\mathbf{s}, t)$ at the reference position $\mathbf{s}$ relative to the moving coordinate system (x_1, x_2, x_3) are described by a set of shape functions $\mathbf{N}(\mathbf{s})$ of dimension $3 \times n$ and the belonging n generalized coordinates

$$\mathbf{u}(\mathbf{s}, t) = \mathbf{N}(\mathbf{s})\mathbf{q}(t) \tag{1}$$

The shape functions represent piecewise polynomial interpolation functions in the FE formulation or linear eigenmodes. These parameters $\bar{\mathbf{x}}_c(t)$, $\boldsymbol{\theta}(t)$ and $\mathbf{q}(t)$ represent the degrees-of-freedom of the floating body. The deformable body inertia can be defined in terms of a set of inertia shape integrals that depend on the assumed displacement field. The use of the mixed set of reference and elastic coordinates leads to a highly nonlinear mass matrix as a result of the inertia coupling between the reference and the elastic displacements.

To circumvent these nonlinearities Kawamoto et al. 1999 suggested an alternative moving frame formulation, which they named the Local Observer Frame formulation. The formulation contains some of the same principles as the standard formulation but no relation between the rigid body motion of the body and the moving frame of reference is postulated. In addition to the elastic deformations the rigid body motion relative to the moving frame must be included in the formulation. Then the displacement vector of a material point is described by

$$\mathbf{u}(\mathbf{s}, t) = \mathbf{N}(\mathbf{s})\mathbf{q}(t) \quad , \quad \mathbf{q}(t) = \begin{bmatrix} \mathbf{q}_r(t) \\ \mathbf{q}_f(t) \end{bmatrix} \tag{2}$$

where $\mathbf{N}(\mathbf{s})$ is a $3 \times (n_r + n_f)$ dimensional interpolation matrix, $\mathbf{q}_r(t)$ is an n_r-dimensional vector describing the rigid body motion. n_r denotes the number of independent rigid modes of the body, i.e. $n_r = 3$ for plane problems and $n_r = 6$ for space problems. $\mathbf{q}_f(t)$ describes the elastic deformations. In this formulation the reference coordinates of the moving frame do not enter as unknown degrees-of-freedom attributed to the moving body. The motion of the moving frame of reference is independent of the motion of the substructure, and determined from an update scheme to prevent the body from floating too far away from the moving frame such that linear theory is adequate. This updating must not necessarily be performed in each time step. The actual degrees of freedom of the body are the generalized coordinates which define the elastic displacements and rigid body motion relative to the moving frame. Hereby, it is not necessary to iterate the mass matrices which reduce the computation time. The updating depends on how the rigid body displacements of the body are selected. In Figure 1a the updated moving frame of reference $(x_{1,s}, x_{2,s}, x_{3,s})$ is determined as a fixed base at the left end where the updating in Figure 1b is based on a connecting line between the end points. In the former case the elastic deformations are clamped to the stiff body motion. In the latter case the elastic deformations are simply supported. The latter case will typically imply smaller elastic deformations and correspondingly reduce the effect of geometrical nonlinearities. Similarly, the kinematical constraints become linear functions of the degrees-of-freedom.

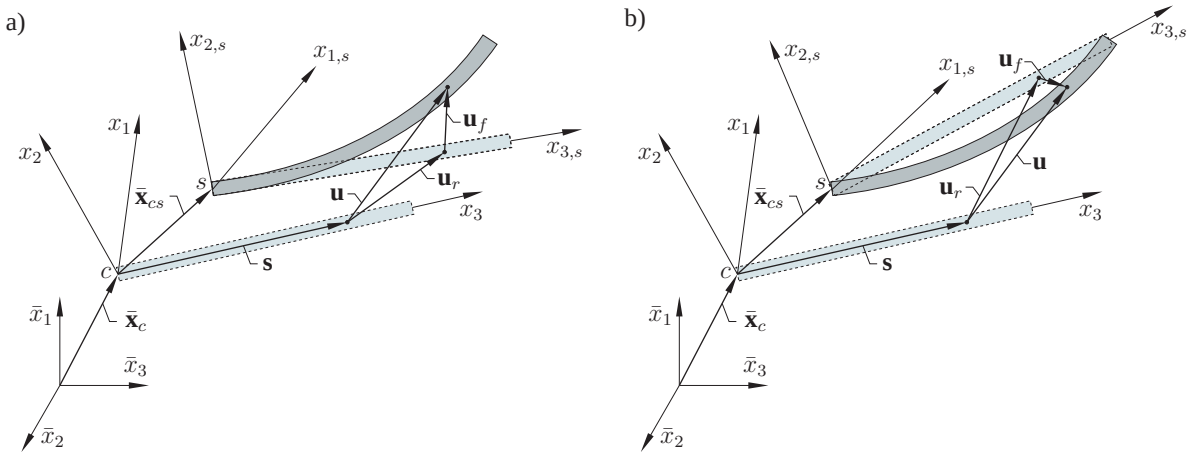

Figure 1. Moving observer frame formulations. a) Clamped elastic deformations. b) Simply supported elastic deformations.

2. EQUATIONS OF MOTION BY USE OF A LOCAL OBSERVER FRAME

$\tilde{\boldsymbol{\omega}}$ denotes the spin matrix of the angular velocity vector $\boldsymbol{\omega}$ and $\mathbf{v}_c$ is the velocity vector of the origin of the moving observer frame. Then the moving frame components of the velocity vector of a material point within the substructure are given as

$$\mathbf{v} = \mathbf{v}_c + \tilde{\boldsymbol{\omega}}(\mathbf{s} + \mathbf{N}\mathbf{q}) + \mathbf{N}\dot{\mathbf{q}} \tag{3}$$

The external loads referred to the shear centre and moments per unit length are assembled in $\bar{\mathbf{p}}(\mathbf{s}, t)$ and $\bar{\mathbf{m}}(\mathbf{s}, t)$, respectively. Typically, these encompass gravity and aerodynamic loads. Some of the components entering the load vector such as the gravity load are most suitably specified in fixed frame coordinates, whereas the aerodynamic loading is specified in moving frame coordinates $\mathbf{p}_A$ and $\mathbf{m}_A$. $\mathbf{p}'_A$ is acting perpendicular and $\mathbf{m}'_A$ tangential to the deformed beam axis. The components are conveniently specified in an auxiliary co-rotated (x'_1, x'_2, x'_3)-coordinate system as $\mathbf{p}'_A$ and $\mathbf{m}'_A$. The corresponding components in moving frame coordinates

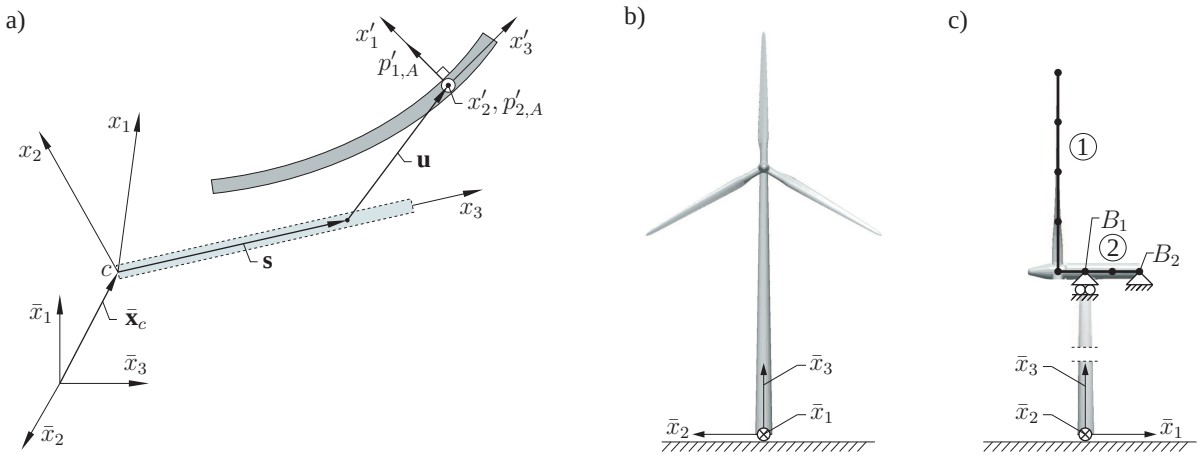

Figure 2. a) Aerodynamic load $\mathbf{p}'_A$ in the deformed beam axis. b) Fixed frame of reference in the wind turbine. c) The numerical example.

become

$$\mathbf{p}_A = \mathbf{R}'\mathbf{p}'_A \quad , \quad \mathbf{m}_A = \mathbf{u} \times \mathbf{p}_A + \mathbf{R}'\mathbf{m}'_A = -\tilde{\mathbf{p}}_A\mathbf{u} + \mathbf{R}'\mathbf{m}'_A = -\tilde{\mathbf{p}}_A\mathbf{N}\mathbf{q} + \mathbf{R}'\mathbf{m}'_A \tag{4}$$

In determining the transformation matrix $\mathbf{R}'(\mathbf{q})$ small rotations are assumed. This will introduce linear parametric excitations and quadratic nonlinearities in the description. Notice that the load description (4) is non-conservative, i.e. no potential function exists.

Constraints are introduced in order to incorporate restrictions on the relative displacements and rotations of the substructures. In relation to a wind turbine the coupling of two substructures can e.g. be of the blade and rotor shaft and internal supports of the rotor shaft are introduced by bearings restricting the displacement from the nacelle, see Figure 2c. All the rotating substructures in a wind turbine rotate around fixed axis relative to each other whereby the rotations can be integrated and the constraints become of the holonomic type. Further, the assumption implies that the constraints become linear

$$\mathbf{\Phi} = \mathbf{B}\mathbf{q} + \mathbf{b} = \mathbf{0} \tag{5}$$

where **B** contains restrictions on the substructure relative to the moving frame of reference and **b** is introduced when restrictions in the fixed frame are formulated e.g. when two substructures are connected. In such cases **b** describes either the global position or global rotation of the moving frame of reference.

The equations of motion are conveniently derived using analytical dynamics based merely on scalar quantities such as the kinetic $T = T(\mathbf{q}, \dot{\mathbf{q}})$ and the potential energy $U = U(\mathbf{q})$ containing contribution from the strain energy and conservative external loads $\mathbf{Q}_c(\mathbf{q})$ such as gravity, in addition to vectorial quantities as the non-conservative loads $\mathbf{Q}_{nc}(\mathbf{q})$. The non-conservative loads are caused by the follower character of the aerodynamic loads. The kinetic energy is most convenient determined by use of the moving frame components of the velocity vector **v** from (3). The resulting constrained equations of motion for the multibody system become

$$\begin{bmatrix} \mathbf{M} & \mathbf{0} \\ \mathbf{0} & \mathbf{0} \end{bmatrix} \begin{bmatrix} \ddot{\mathbf{q}} \\ \ddot{\boldsymbol{\lambda}} \end{bmatrix} + \begin{bmatrix} 2\mathbf{G} & \mathbf{0} \\ \mathbf{0} & \mathbf{0} \end{bmatrix} \begin{bmatrix} \dot{\mathbf{q}} \\ \dot{\boldsymbol{\lambda}} \end{bmatrix} + \begin{bmatrix} \mathbf{K} + \dot{\mathbf{G}} + \mathbf{D} & \mathbf{B}^T \\ \mathbf{B} & \mathbf{0} \end{bmatrix} \begin{bmatrix} \mathbf{q} \\ \boldsymbol{\lambda} \end{bmatrix} = \begin{bmatrix} -\mathbf{M}_0^T\mathbf{a}_c - \dot{\mathbf{J}}_0^T + \mathbf{J}_2^T + \mathbf{Q}_c(\mathbf{q}) + \mathbf{Q}_{nc}(\mathbf{q}) \\ -\mathbf{b} \end{bmatrix} \tag{6}$$

where **K** is the elastic stiffness matrix and

$$\mathbf{M} = \int_V \mathbf{N}^T\mathbf{N}\rho dV \quad , \quad \mathbf{M}_0 = \int_V \mathbf{N}\rho dV \quad , \quad \mathbf{D} = \int_V \mathbf{N}^T\tilde{\boldsymbol{\omega}}\tilde{\boldsymbol{\omega}}\mathbf{N}\rho dV \tag{7}$$

$$\mathbf{G} = \int_V \mathbf{N}^T\tilde{\boldsymbol{\omega}}\mathbf{N}\rho dV \quad , \quad \mathbf{J}_0 = \boldsymbol{\omega}^T\int_V \tilde{\mathbf{s}}\mathbf{N}\rho dV \quad , \quad \mathbf{J}_2 = \boldsymbol{\omega}^T\int_V \tilde{\mathbf{s}}\tilde{\boldsymbol{\omega}}\mathbf{N}\rho dV \tag{8}$$

The Lagrange multiplier vector $\boldsymbol{\lambda}$ stores the forces and moments acting at the kinematical constraints. **M** is the conventional symmetric mass matrix of the body in the moving frame of reference. $\mathbf{M}_0$ is representing the effect of uniform translation. The effect of centrifugal forces are contained in the symmetric matrix **D** and the gyroscopic forces are represented by the skew symmetric matrix **G**. The remaining **J**-terms are couplings between the reference position and the shape functions. The equations of motion (6) is solved by means of a Newmark algorithm with $(\beta, \gamma) = (\frac{1}{4}, \frac{1}{2})$. Because the constraints in principle introduce infinite stiffness into the system it becomes necessary to apply unconditional stable time integrators. The energy conser-

vation of the indicated Newmark scheme is only guaranteed for linear systems. In the present version of the algorithm $\mathbf{Q}_c(\mathbf{q})$ and $\mathbf{Q}_{nc}(\mathbf{q})$ are simply determined by use of the previous calculated $\mathbf{q}$. To avoid large deviations relatively small time steps are used corresponding to 150 per period of the lowest eigenvibration. The size of the time steps can be increased by use of iterations in the equation of motion.

3. UPDATE OF MOVING FRAME OF REFERENCE

Whenever the moving substructure has drifted too far away from the moving observer frame the latter is updated to coincide with the present position and orientation of the fictitious stiff body $(x_{1,s}, x_{2,s}, x_{3,s})$-coordinate system shown in Figure 1a and Figure 1b. The new position, velocity and acceleration of the updated origin in fixed frame coordinates are

$$\bar{\mathbf{x}}_s = \bar{\mathbf{x}}_c + \bar{\mathbf{x}}_{cs} = \bar{\mathbf{x}}_c + \mathbf{R}_c\mathbf{u}(0) \quad , \quad \bar{\mathbf{v}}_s = \bar{\mathbf{v}}_c + \dot{\mathbf{R}}_c\mathbf{u}(0) + \mathbf{R}_c\dot{\mathbf{u}}(0) \tag{9}$$

$$\bar{\mathbf{a}}_s = \bar{\mathbf{a}}_c + \ddot{\mathbf{R}}_c\mathbf{u}(0) + 2\dot{\mathbf{R}}_c\dot{\mathbf{u}}(0) + \mathbf{R}_c\ddot{\mathbf{u}}(0) \tag{10}$$

where $\mathbf{u}(0)$ is the rigid body displacement at $\mathbf{s} = \mathbf{0}$ and $\mathbf{R}_c$ is the rotation matrix from the moving frame (x_1, x_2, x_3) to the fixed frame $(\bar{x}_1, \bar{x}_2, \bar{x}_3)$. Next, the orientation, angular velocity and angular acceleration of the updated moving frame are determined from the following Taylor expansion type of extrapolations

$$\boldsymbol{\theta}_s = \boldsymbol{\varphi}(0) + \boldsymbol{\omega}_c\Delta t + \tfrac{1}{2}\boldsymbol{\alpha}_c\Delta t^2 \quad , \quad \boldsymbol{\omega}_s = \dot{\boldsymbol{\varphi}}(0) + \boldsymbol{\omega}_c + \boldsymbol{\alpha}_c\Delta t \quad , \quad \boldsymbol{\alpha}_s = \ddot{\boldsymbol{\varphi}}(0) + \boldsymbol{\alpha}_c \tag{11}$$

where $\boldsymbol{\varphi}(0)$, $\dot{\boldsymbol{\varphi}}(0)$ and $\ddot{\boldsymbol{\varphi}}(0)$ are the rotation, angular velocity and angular acceleration of the rigid body rotation at $\mathbf{s} = \mathbf{0}$ and Δt is the time increment. These rotations are determined from the generalized degrees-of-freedom $\mathbf{q}$, $\dot{\mathbf{q}}$ and $\ddot{\mathbf{q}}$. $\mathbf{R}_s(\boldsymbol{\theta}_s)$ can then be determined and the rotation matrix to the fixed frame of reference become $\mathbf{R} = \mathbf{R}_c\mathbf{R}_s$. $\boldsymbol{\omega}_s$ and $\boldsymbol{\alpha}_s$ are converted into spin matrices and used in (6) for the next time step. In (9) and (10) both $\dot{\mathbf{R}}_c$ and $\ddot{\mathbf{R}}_c$ enter which are determined by

$$\dot{\mathbf{R}}_c = \mathbf{R}_c(\tilde{\boldsymbol{\omega}}_c + \tilde{\boldsymbol{\alpha}}_c\Delta t) \quad , \quad \ddot{\mathbf{R}}_c = \mathbf{R}_c(\tilde{\boldsymbol{\alpha}}_c - \dot{\mathbf{R}}_c^T\dot{\mathbf{R}}_c) \tag{12}$$

When the updating of the moving frame is performed all rigid body motions are initialized with zero.

4. NUMERICAL EXAMPLE

In this section the theory is illustrated with a simplified system with 2 substructures and kinematic constraints as shown in Figure 2c. The coordinate axes both start at the hub with the moving frame coordinate axis x_3 pointing in the longitudinal direction of the respective beam structures. The blade and shaft are connected at the hub whereby the displacements and rotations of the two substructures at this point are equal. Moreover, the shaft is supported by two bearings B_1 and B_2 where B_1 allows displacements in the longitudinal direction and all displacements are fixed at B_2. The length of the blade is $L = 46\,\mathrm{m}$ with a total weight of 10 t and it is constructed by NACA 63-418 section profiles. The cross section parameters and the mass distribution throughout the blade are presented in Larsen & Nielsen [6]. The numerical FE-model is based on prismatic Bernoulli-Euler beam elements accounting for shear and St. Venant torsion with 6 degrees-of-freedom for each node. The rotor shaft has a length of $L = 4\,\mathrm{m}$ and

diameter of $d = 0.4\,\mathrm{m}$ and the bearing B_1 is placed in the centre and B_2 at the most far end from the blade. The shaft has constant geometry and material parameters and is modelled with the same type of element as the blade model. The following displacement constraints $\mathbf{\Phi}_d$ and rotation constraints $\mathbf{\Phi}_r$ defined in the fixed frame of reference are introduced to couple the two substructures

$$\mathbf{\Phi}_d = \mathbf{R}_1\mathbf{u}_1(0) + \bar{\mathbf{x}}_{c1} - \left(\mathbf{R}_2\mathbf{u}_2(0) + \bar{\mathbf{x}}_{c2}\right) = \mathbf{R}_1\mathbf{N}_1(0)\mathbf{q}_1 + \bar{\mathbf{x}}_{c1} - \left(\mathbf{R}_2\mathbf{N}_2(0)\mathbf{q}_2 + \bar{\mathbf{x}}_{c2}\right) = \mathbf{0} \quad (13)$$

$$\mathbf{\Phi}_r = \mathbf{R}_1\boldsymbol{\varphi}_1(0) + \bar{\boldsymbol{\theta}}_1 - \left(\mathbf{R}_2\boldsymbol{\varphi}_2(0) + \bar{\boldsymbol{\theta}}_2\right) = \mathbf{R}_1\mathbf{P}_1(0)\mathbf{q}_1 + \bar{\boldsymbol{\theta}}_1 - \left(\mathbf{R}_2\mathbf{P}_2(0)\mathbf{q}_2 + \bar{\boldsymbol{\theta}}_2\right) = \mathbf{0} \quad (14)$$

where $\bar{\mathbf{x}}_c$ and $\bar{\boldsymbol{\theta}}$ are the fixed frame position of the moving frame origin and accumulated rotation-parameter of the moving frame, respectively. The constraints are introduced in the system of equation as described in (5). As seen, the constraints become linear in the degrees of freedom $\mathbf{q}_1$ and $\mathbf{q}_2$ related to the 2 substructures. The displacement constraints for the two bearings do not need to be formulated in the fixed frame because they are not linked to other substructures. The constraints for the bearing B_2 become

$$\mathbf{\Phi}_{B_2} = \mathbf{u}_2(L_2) = \mathbf{N}_2(L_2)\mathbf{q}_2 = \mathbf{0} \quad (15)$$

and similar with the bearing B_1 where only the components in the direction orthogonal to the beam axis enter. Due to the homogeneity and small deformations the shaft substructure is in the following simulations modelled merely by 4 beam elements, whereas 20 elements are used for the non-homogeneous blade. The reduced model of the blade is based on undamped eigenmodes $\mathbf{\Phi}_e$ determined from the belonging consistent mass matrix $\mathbf{M}$ and the stiffness matrix $\mathbf{K}$ from the following eigenvalue problem

$$\left(\mathbf{K} - \omega^2\mathbf{M}\right)\mathbf{\Phi}_e = \mathbf{0} \quad (16)$$

where the kinematic constraints to the fictitious stiff body motion have been included. The rigid body modes are next added to $\mathbf{\Phi}_e$ to have a full description of displacements and rotations at the nodes. In the reduced model the shaft substructure is kept as an FE-model similar to the model where both the blade and shaft are based on finite elements. The updating of the moving frame is performed in each time step.

To demonstrate the multibody formulation a linearly increasing tip load is applied in both the blade and edge directions during the first 3 s. The loads are then removed and the response and the angular velocity Ω are observed in Figure 3a. Here, it is seen that the response from the FE-model and reduced model are almost identical with 16 elastic modes. Several of them especially those dominated by torsion around the longitudinal direction are not important. In Figure 3b Ω is plotted for the two models and it is observed that they also are identical. It is chosen to load up in the edge direction to end up at approximately $\Omega = 1.6\,\mathrm{rad/s}$ which is the nominal velocity for this the considered turbine. It is also observed that Ω is almost constant which is a sign of energy conservation. Next, the influence of introducing the non-linear correction on the load from (4) is examined. This is done by applying a load at the tip of the blade in the deformed blade direction i.e. $p'_{1,A}$. To examine when this correction has an influence the tip load is increased linearly during the first 2 s of the simulation and then removing the load to examine eigenvibrations of the system. In Figure 4a it is seen that deviations between the two loading methods are first visible at $u_{f,1}/L \approx 0.09$ where the response from the non-linear correction becomes the largest. The reason for the larger displacement with the non-linear

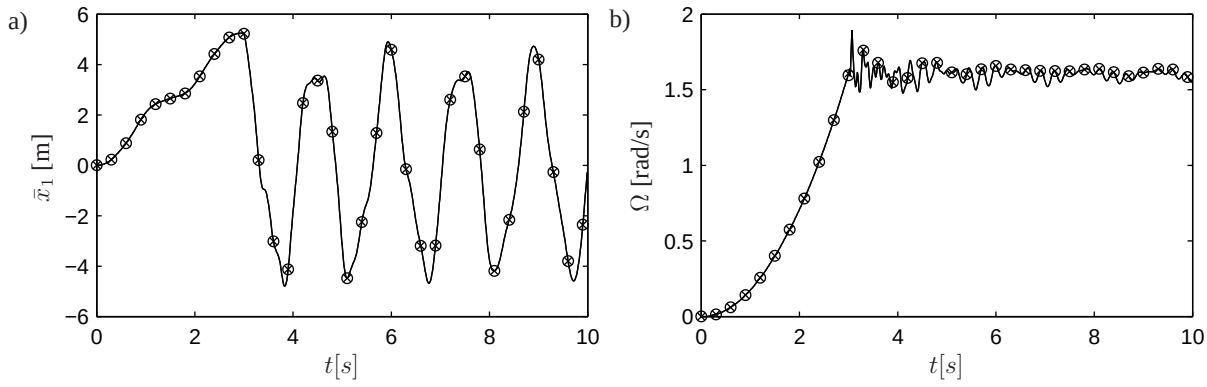

Figure 3. a) Tip displacement in the global $\bar{x}_1$-direction. b) Angular velocity of the rotor. $(\times)$ FE-model. $(\circ)$ converged reduced model.

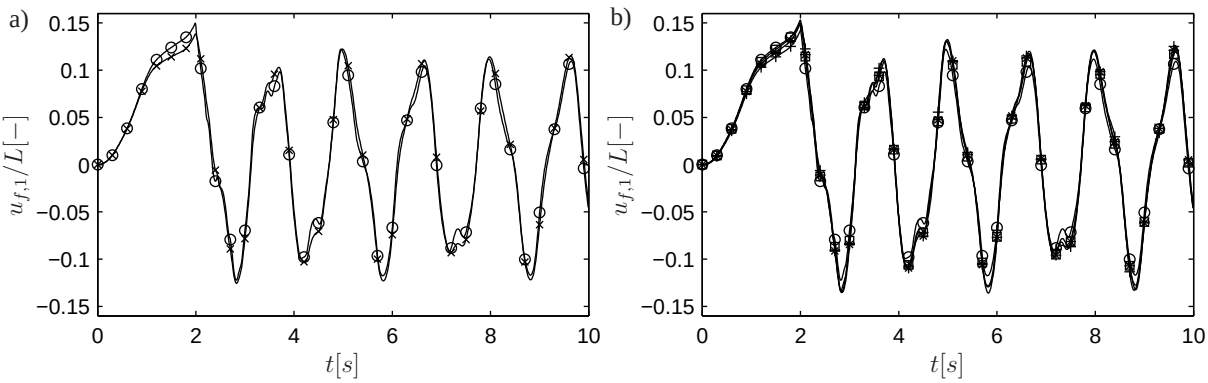

Figure 4. a) Normalized elastic tip displacement for FE-model. $(\times)$ linear applied tip load. $(\circ)$ non-linear applied tip load. b) Normalized elastic tip displacement for non-linear applied tip load. $(\circ)$ FE-model. $(+)$ 3 modes. $(*)$ 5 modes. $(\square)$ 10 modes.

correction is mainly due to the moment contribution which is not present when applying the load in linear theory. Increasing the load further results in larger deviations and therefore, it is chosen to cut off the load at $u_{f,1}/L \approx 0.15$. In the remaining part of the simulation the outcome of the different motions at $t = 2$ s is visible. In Figure 4b it is seen that for $n_f = 10$ the response is very much alike to the FE-model during the loading stage. By use of 3 and 5 modes the response is predicted to be smaller. It can hereby be concluded that by use of the non-linear load correction for large tip deflections it is necessary with 10 modes but to describe eigenvibrations 3 modes are sufficient. Next, the influence of using the moving frame formulation based on simple supported elastic deformations illustrated in Figure 1b are investigated for the same non-linear applied tip load as before. A 3rd formulation is investigated, where the simple support at the tip is placed at the 3/4 point. In both cases the axial rotation component is fixed at the hub when determining the elastic modes. In Figure 5a it is seen that by use of the simple supports the response during the loading stage is reduced compared to the fixed models also used in Figure 4b but overall the response is very similar. However, as anticipated the displacements presented in Figure 5b from the moving frame is significantly reduced by using these types of elastic modes making linear theory more reasonable.

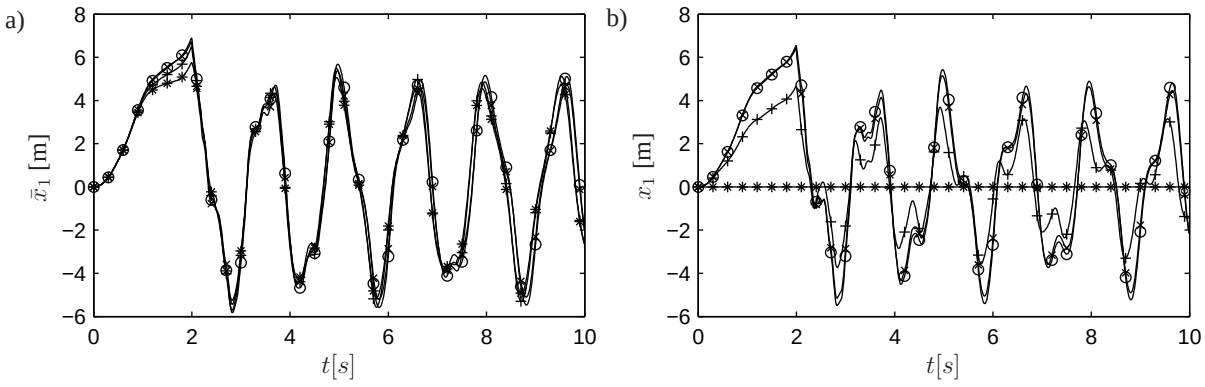

Figure 5. Tip displacement for a non-linear applied tip load. a) Fixed frame coordinate. b) Moving frame coordinates. $(\times)$ FE-model with fixed base. $(\circ)$ reduced model with fixed base. $(+)$ reduced model with simple support at the 3/4 point. $(*)$ reduced model with simple supports at the end points.

5. CONCLUSIONS

By use of a multibody formulated where the motion of the moving frame of reference is predicted the equations of motion become linear, contrary to the standard multibody formulation where iterations are necessary. Moreover, it is only necessary to update the moving frame of reference when the body is displaced to far away that linear theory is adequate which speeds up the simulations further. To account for loads being applied in the deformed position a nonlinear correction has been implemented. It is shown that an effect of this correction first is visible at $u_f/L \approx 0.09$ compared to appliying the load in the undeformed position. The reduced model of the blade performs in most situations identical to the full FE-model of the blade. However, when the nonlinear load correction is applied a larger amount of elastic modes are necessary due to the more complex deflections which are not sufficiently described by the lowest 3-5 elastic modes. By use of elastic modes which better describe the response it is also possible to reduce the overall displacements from the moving frame. In an upcoming work a more realistic load model will be incorporated together with a criteria for when the moving frame of reference should be updated i.e. based on a certain deflection of the tip from the moving frame.

6. ACKNOWLEDGEMENTS

This work has been supported by the Danish Council for Strategic Research through the project 'Nonlinear Multibody Dynamics of Wind Turbines'.

REFERENCES

[1] P.E. Nikravesh, *Computer-aided Analysis of Mechanical Systems*, Prentice-Hall 1988.

[2] J.G. de Jalon & E. Bayo, *Kinematic and Dynamic Simulations of Multibody Systems - The Real-Time Challenge*, Springer-Verlag 1993.

[3] M. Géradin & A. Cardona, *Flexible Multibody Dynamics - A Finite Element Approach*, John Wiley & Sons Ltd 2001.

[4] A.A. Shabana, *Dynamics of Multibody Systems*, Third Edition, Cambridge University Press 2005.

[5] A. Kawamoto, M. Inagaki, T. Aoyama and K. Yasuda, "Vibration of Moving Flexible Bodies (Formulation of Dynamics by using Normal Modes and a Local Observer Frame)", *Proceeding of DETC99/VIB-8232*, 1999.

[6] J.W. Larsen and S.R.K. Nielsen (2006a), "Non-Linear Dynamics of Wind Turbine Wings", *Journal of Non-Linear Mechanics*, **41**, 629–643.